Biochimica et Biophysica Acta, 1063 (1991) 137–146

ADONIS 000527369100145A

BBAMEM 75177

Functional size of complement and perforin pores compared by confocal laser scanning microscopy and fluorescence microphotolysis

Heinrich Sauer [1], Lothar Pratsch [1], Jürg Tschopp [2], Sucharit Bhakdi [3] and Reiner Peters [1,4]

[1] *Max-Planck-Institut für Biophysik, Frankfurt (F.R.G.),* [2] *Institut für Biochemie, Universität Lausanne, Epalinges (Switzerland),* [3] *Institut für Medizinische Mikrobiologie, Johannes Gutenberg-Universität Mainz, Mainz (F.R.G.) and* [4] *Institut für Medizinische Physik, Wilhelms-Universität, Münster (F.R.G.)*

(Received 3 October 1990)

Key words: Pore size; Perforin pore; Confocal laser scanning microscopy; Fluorescence microphotolysis

Confocal laser scanning microscopy and fluorescence microphotolysis (also referred to as fluorescence photobleaching recovery) were employed to study the transport of hydrophilic fluorescent tracers through complement and perforin pores. By optimizing the confocal effect it was possible to determine the exclusion limit of the pores in situ, i.e. without separation of cells and tracer solution. Single-cell flux measurements by fluorescence microphotolysis yielded information on the sample population distribution of flux rates. By these means a direct comparison of complement and perforin pores was made in sheep erythrocyte membranes. In accordance with previous studies employing a variety of different techniques complement pores were found to have a functional radius of approx. 50 Å when generated at high complement concentrations. The flux rate distribution indicated that pore size heterogeneity was rather small under these conditions. Perforin pores, generated in sheep erythrocyte membranes at high perforin concentrations, were found to have a functional size very similar to complement pores. Furthermore, the functional size of the perforin pore seemed to be relatively independent of the dynamic properties of the target membrane since in two cell membranes which are very different in this regard, the human erythrocyte membrane and the plasma membrane of erythroleukemic cells, the functional radius of the perforin pore was also close to 50 Å. A perforin-specific antibody reduced the functional radius of perforin pores to 45 Å.

Introduction

Immunological defense as well as cellular attack processes frequently involve the action of proteins that form pores in the plasma membrane of target cells (for review, see Ref. 1). A single functional lesion is sufficient to induce swelling and finally colloid osmotic lysis of erythrocytes [2]. The terminal C5b-9 complement complex and lymphocyte perforin (cytolysin) are two well-studied prototypes of pore-formers. The transmembrane complement pore is formed from C5b-8 monomers to which multiple C9 molecules are bound [3]. Perforin is a 66 kDa protein [4,5] that occurs in cytoplasmic granules of large granular lymphocytes and cytolytic T-lymphocytes. Purified perforin binds spontaneously to cellular and artificial membranes containing phosphatidylcholine [6]. Subsequent to membrane binding the pore is formed by assembly of about 15 monomers [7] into a cylindrical structure. Recent molecular genetic work has revealed [8–10] that C7, C8, C9 and perforin harbor domains of high homology. Apparently [11] these proteins have a common core with lipid binding and polymerization activities as well as differentiated domains with specialized functions such as C5 binding.

Functional and structural properties of complement pores have been studied previously by osmotic protection [12,13], marker release [14,15], efflux kinetics [16,17], electric single channel recording [18–20], and electron microscopy [21,22]. Perforin pores have been predominantly studied by electron microscopic techniques [23] although some functional studies are also available [24–26]. Altogether these studies suggest (see also the Discussion and Table IV) that both complement and perforin, at sufficiently high concentrations,

Correspondence: R. Peters, Max-Planck-Institut für Biophysik, Heinrich-Hoffmann-Strasse 7, D-6000 Frankfurt 71, F.R.G.

form large cylindrical pores which perpendicularly travers the plasma membrane of the target cells. The internal radius of the complement pore apparently assumes an upper limiting value of about 50–55 Å at high C9 concentrations [21]. Results for the size of perforin pores are more heterogeneous. It is widely believed, however, that, at least at high perforin concentrations, the radius of the perforin pore is substantially larger than 50 Å.

Recently, laser-based microscopic techniques have provided new access to the study of molecular distribution and transport in single cells. Confocal laser scanning microscopy (CLSM) (for review, see [27,28]) has advanced to a stage that approaches the theoretical resolution limit. The gain in spatial resolution is moderate in the focal (x-y-) plane but rather dramatic in the direction of the optical (z-) axis where a resolution of about 0.4 μm has been experimentally verified [28]. Photobleaching techniques, initially devised [29–32] for studying the lateral mobility of proteins and lipids in membranes, have been extended [33] to single-cell flux measurements. In contrast to conventional methods for the measurement of membrane transport, single-cell flux measurements yield not only average values of transport coefficients but also their sample population distribution. We have recently extended such flux measurements from the single-cell to the single-channel level [34] by measuring the flux of the fluorescent probe Lucifer Yellow through single perforin pores.

Our fluorescence microscopic single-channel recordings suggested [34] that the functional radius of the perforin pore in human erythrocyte membranes is independent of the perforin concentration within wide limits. The value of the functional pore radius, however, could be only roughly estimated because the transport of only one tracer, Lucifer Yellow, had been measured. In the present study the functional size of the perforin pore was analysed in more detail and directly compared with the size of complement pores. Complement or perforin pores were generated in the same membrane system, i.e. resealed sheep erythrocyte ghosts, employing concentrations of pore-forming proteins 40–80 times larger than required for 50% lysis. The exclusion limit and the flux rates were determined for a series of fluorescent tracers including Lucifer Yellow and fluorescently labeled Dextrans of 1–70 kDa mean molecular mass. For perforin such measurements were also performed with human erythrocyte ghosts and intact erythroleukemic cells. Our results suggest that the maximum size of complement and perforin pores is similar and possibly independent of the target membrane.

Materials and Methods

Fluorescent tracers

The series of membrane-impermeant hydrophilic fluorescent tracers included Lucifer Yellow and fluorescein-labeled Dextrans of approx. 1 kDa (FD1), 4 kDa (FD4), 10 kDa (FD10), 20 kDa (FD20), 40 kDa (FD40), and 70 kDa (FD70) mean molecular mass. Lucifer Yellow (LY), FD10, FD20, FD40, and FD70 were obtained from Sigma, Deisenhofen, F.R.G. FD1 and FD4 were prepared by labelling a 1kDa- and a 4kDa-Dextran (both from Serva, Heidelberg, F.R.G.) with FITC according to DeBelder and Granath [35]. The molecular masses, lateral diffusion coefficients as measured by the fluorescence microphotolysis technique, and the hydrodynamic (Stokes') radii of these molecules as derived from the diffusion coefficients are listed in Table I.

TABLE I

Diffusion coefficients and stokes' radii of fluorescent tracers

Tracer	Mean molecular mass (kDa)	Diffusion coefficient, D (10^{-8} cm^2 s^{-1})	Stokes' radius, a (Å)
LY	0.457	274.9	7.8
FD1	0.9–1.2	134.2	16.0
FD4	4.0–6.0	88.8	24.2
FD10	10.5	75.7	28.3
FD20	17.5	65.1	33.0
FD40	41.0	46.3	46.4
FD70	62.0	39.0	55.1

Resealed erythrocyte ghosts

Human blood was obtained from the Blutspendedienst Hessen (a local blood bank). Sheep blood was purchased from Flow Laboratories, Meckenheim, F.R.G. Resealed ghosts were prepared from erythrocytes according to a modification [15] of the methods devised by Schwoch and Passow [36]. In short, cells were washed three times in phosphate-buffered saline (pH 7.4) and taken up in Hepes buffer (10.0 mM Hepes, 137 mM NaCl, 10 mM glucose, 5.3 mM KCl, 0.39 mM K_2HPO_4, 0.337 mM Na_2HPO_4) to yield a 50% (vol/vol) suspension. 1 volume of the cell suspension was cooled to 0 °C and mixed with 17 volumes of an ice-cold Mg^{2+} acetate solution (4 mM $MgCl_2$, 3.5 mM acetic acid, pH 6.4). The pH was titrated to 6.0 with acetic acid. After 5 min at 0 °C isotonicity was restored by the addition of 2.4 volumes of a 10-fold concentrated Hepes buffer and 2.4 volumes of a Ca^{2+}/Mg^{2+} solution (13 mM $CaCl_2$, 8 mM $MgSO_4$). The pH was adjusted to 7.4 with 0.1 M NaOH. After five further minutes at 0 °C the cell suspension was incubated for 50 min at 37 °C (resealing) and then washed with the Hepes buffer.

K-562 cells

K-562 cells, an established myeloleukemia cell line [37], were obtained from the American Tissue Culture Collection and maintained in RPMI 1640 medium

(Gibco, Karlsruhe, F.R.G.) supplemented with 10% fetal calf serum and 4 mM glutamine.

Generation of complement and perforin pores

Human lyophilyzed complement serum was purchased from Sigma, Deisenhofen, F.R.G. and taken up in destilled water as prescribed. Antiserum against the Forssman antigen was from Cordis Laboratories, Miami, FL, U.S.A. Lytic granule proteins were isolated from the murine T cell clone B 6.1 by Percoll-density centrifugation [4]. The preparation and characterization of the polyclonal perforin-specific antibody used in this study have been described by Tschopp et al. [38].

Complement pores were generated in sheep erythrocyte membranes by incubating resealed sheep erythrocyte ghosts at first with anti-Forssman-antibody (diluted 800-fold). Then, 100 μl of antibody-coated sheep erythrocyte ghosts ($5 \cdot 10^8$ ghosts/ml) were mixed with 400 μl of human complement serum diluted 300-fold with the Hepes buffer containing 1.3 mM $CaCl_2$. The sample was adjusted to 750 μl with $CaCl_2$-supplemented Hepes buffer and incubated for 30 min at 37°C. Ghosts were pelleted and resuspended in 50 μl $CaCl_2$-supplemented Hepes buffer. Thus, the dilution of complement in the reaction mixture was 563-fold. For a 50% lysis of sheep erythrocytes a 32-fold smaller complement concentration (18000-fold dilution) was required. Perforin pores were generated in sheep or human erythrocyte membranes in the following manner. 5 μl of a solution of lytic granule proteins containing 1 μg perforin per ml was diluted 20-fold with Tris-buffered saline (10 mM Tris-HCl, 150 mM NaCl, 1 mM EDTA, 0.1% (w/v) BSA, pH 7.4). 50 μl of the diluted granule protein solution was mixed with 150 μl of a suspension of resealed ghosts ($1 \cdot 10^8$ cells per ml) in Hepes buffer containing 5 mM $CaCl_2$. This was incubated for 15 min at 37°C and then washed twice with Tris-buffered saline. Thus, the dilution of granule proteins in the reaction mixture was 80-fold. For a 50% lysis of both sheep and human erythrocytes a 80-fold smaller perforin concentration (6400-fold dilution) was required.

A two-step procedure was employed for generating perforin pores in the plasma membrane of K-562 cells in order to avoid or reduce internalisation or other elimination of perforin by the cells. In the first step the temperature was kept at 0°C, perforin binds to the cell surface but does not polymerise to form pores [26]. In the second step the temperature was increased to 37°C thus inducing pore formation, flux measurements were performed shortly (10 min) after raising the temperature. In detail, K-562 cells were suspended in Hepes buffer containing 5 mM $CaCl_2$ and 0.3 mM $MgSO_4$ at $1 \cdot 10^5$ cells/ml. 150 μl of the cell suspension was kept on ice and mixed with 10 μl of a 6-fold dilution of lytic granule proteins. The sample was incubated for 30 min at 0°C. Cells were gently pelleted at 0°C and resuspended in Hepes buffer supplemented with 1.3 mM $CaCl_2$ and 0.25 mM of a 110 kDa Dextran (to inhibit colloid osmotic lysis).

It may be noted that comparatively high concentrations of both complement and perforin were employed in the present study. The relationship between the degree of cell lysis and complement or perforin concentration has been studied previously by microfluorimetric measurements [34] and CLSM scans (Sauer et al., unpublished results). The degree of lysis is defined here as the fraction of cells which become permeable to small fluorescent tracers such as Lucifer Yellow or FD1, i.e. the fraction of cells which carry at least one pore.

Laser scanning microscopy and flux measurements

Resealed ghosts or K-562 cells, treated with complement or perforin as described, were incubated with one of the fluorescent tracers (final concentration 0.1 mg/ml). The cell suspension was placed in a flat glas capillary (microslide, Camlab, Cambridge, U.K., path length 50 μl). The microslide was mounted on a regular slide and sealed with silicon grease.

The confocal laser scanning microscope of Wild Leitz Instruments (Heidelberg, F.R.G.) was employed. Usually a 100-fold oil-immersion objective with a numerical aperture of 1.3 was used. The confocal aperture could be continuously varied over an arbitrary scale ranging from 0 to 255. A scan with a resolution of 256×512 pixels could be taken in approx. 1 s and the number of scans to be made in succession and averaged could be set by software. All CLSM studies were performed at ambient temperature (approx. 23°C).

Flux measurements were performed with the photobleaching apparatus described by Peters and Scholz [39] consisting of a small argon ion laser, an inverted fluorescence microscope with photometric attachment, a single-photon counter, a small computer, and several optical components. An acousto-optical modulator [40] was employed to alternate between the small average beam power (approx. 100 nW) needed for fluorescence measurement and the high average power (approx. 1 mW) needed for photolysis. An objective with a numerical aperture of 1.3 was used to focus the laser beam into the internal compartment of single ghosts or cells adhering to the upper glass/water interface. An aperture in the path of the laser beam limited the illuminated field to a circle of 2 μm radius. Under these conditions the depth of focus is approximately 2 μm [41]. Flux measurements were initiated by recording the fluorescence of the internal cell compartment employing a small beam power. The internal compartment was then partially depleted of fluorescence by a high-intensity laser pulse, and influx of fluorescent tracer from the external compartment into the ghost or cell was followed by fluorescence measurement at the initial low beam power.

The single-cell flux rate k was derived by fitting Eqn. 1 [33] to the measured fluorescence recovery:

$$f = [F(t) - F(\infty)]/[F(0) - F(\infty)] = e^{-kt} \quad (1)$$

where f is the fractional fluorescence recovery, and $F(0)$, $F(t)$ and $F(\infty)$ is fluorescence immediately, at time t, and very long after photolysis, respectively. Control experiments showed that ghosts which had not been treated with complement or perforin were perfectly impermeable for the fluorescent tracers. All flux measurements were performed at ambient temperature (approx. 23°C).

Results

The exclusion limit of complement and perforin pores

Confocal laser scanning microscopy is distinguished by its ability to produce thin optical sections. Depending on parameters such as the numerical aperture of the objective, the radius of the illuminated field and the radius of the confocal aperture the effective thickness of the optical section can assume values of approximately ≥ 0.4 μm [28]. We reasoned that this feature should make it possible to visualize and quantitate fluorescence inside single cells even if these were suspended in a thick layer of a strongly fluorescent solution. This was tested with resealed ghosts suspended in a solution of FD70 (thickness of the layer 50 μm). CLSM scans were evaluated for $F_{I/O}$, the ratio of intracellular over extracellular fluorescence. Using an objective with a large numerical aperture (1.3) and a small confocal aperture (≤ 100 on the arbitrary scale, see Materials and Methods) $F_{I/O}$ was found to be 0.10–0.16 for human and 0.15–0.25 for sheep ghosts, respectively. Reduction of the confocal aperture did not reduce $F_{I/O}$. However, increasing the size of the confocal aperture to its maximum (255 on the arbitrary scale) increased $F_{I/O}$ to 0.30 and 0.60, respectively. Thus, intracellular fluorescence could be recorded with little interference from extracellular fluorescence if, and only if, the confocal aperture was optimized for efficient optical sectioning. The small difference in $F_{I/O}$ between human and sheep erythrocyte ghosts may be due to their different thickness. In any event, both human and sheep erythrocytes are particularly small cells with average volumes of approx. 90 fl [42] and 45 fl [43], respectively.

The possibility to measure the intracellular fluorescence of ghosts suspended in fluorescent solutions was used to determine the exclusion limit of complement and perforin pores. Resealed sheep erythrocyte ghosts, treated with a high concentration of complement as described, were incubated with one of the fluorescent tracers listed in Table I. In fluorescence scans (Figs. 1A–E, left) ghosts were clearly visible if the tracer was a fluorescently labeled Dextran with a mass of ≥ 40 kDa.

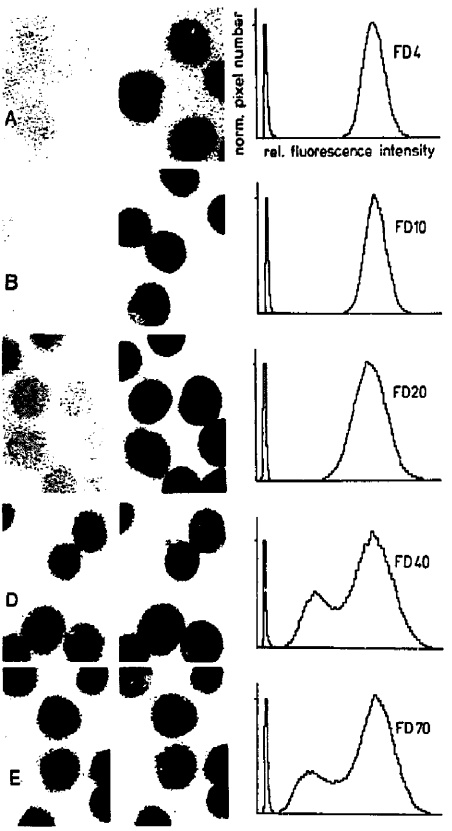

Fig. 1. Exclusion limit of the complement pore. Resealed sheep erythrocyte ghosts were treated with complement and then incubated with FD4 (A), FD10 (B), FD20 (C), FD40 (D), or FD70 (E), respectively, as described in the text. Fluorescence scans were obtained by CLSM before (left) and after (middle) photobleaching. The histograms on the right-hand side represent intensity distributions of the CLSM scans on the left-hand side. The scans and the histograms demonstrate that ghosts are permeable for FD4, FD10 and FD20 but impermeable for FD40 and FD70. In the histograms the peak on the left originates from dark counts, the peak in the center (only D and E) originates from ghosts, while the peak on the right originates from the intensity of the medium (note that only the position of these peaks on the abscissa is significant; the height of the peaks depends on the area density of ghosts). Note that a small degree of bleaching was already introduced by the first scan so that even perfectly permeable ghost appeared slightly darker than background (A–C, left side).

For the smaller Dextrans and for Lucifer Yellow the ghosts were permeable and therefore could hardly be discriminated against the medium. However, even perfectly permeable ghost always appeared a little darker than background, cf Figs. 1A–C left side, 2A–C left side. This was due to a small degree of bleaching by the first scan. The permeable ghosts could be made clearly visible by taking 10 scans in succession at 10-fold increased laser power (Figs. 1A–E, center). By this the

total scanned area was bleached and permeable ghosts showed up because tracer diffusion in free solution was much faster than tracer flux through membrane pores. The visual impression of tracer exclusion given by the scans was quantitated by generating histograms of the intensity distributions (Figs. 1A–E, right). No dependence of the exclusion limit on the incubation time was noted. Even after a 24 h incubation the 40 kDa Dextran was still perfectly excluded by all of the ghosts. The exclusion limit of the perforin pore was determined in the very same manner (Fig. 2). As in the case of complement the 40 kDa Dextran and larger dextrans were strictly excluded without notable dependence on the incubation time (up to 24 h). These results suggested that the effective radius of both complement and perforin pores is equal to or smaller than that of the 40 kDa Dextran.

Permeability of complement and perforin pores in erythrocyte membranes

The permeability of complement and perforin pores was quantitated by flux measurements. Ghosts were treated with complement or perforin and equilibrated with FD10 or one of the smaller tracers. In the fluorescence microphotolysis apparatus a ghost was selected and its intracellular fluorescence was quickly bleached by a short illumination with a high-power laser beam. Then, the influx of fresh tracer was monitored by continuous measurements of the intracellular fluorescence. Typical examples of such measurements for both complement and perforin are displayed in Fig. 3 showing that influx kinetics strongly depended on the molecular size of the tracer.

Conceivably, laser illumination as employed in flux measurements could induce thermal and/or photochemical effects (for review, see Ref. 39) affecting complement or perforin pores. In order to check for this possibility individual ghosts were subjected to repetitive flux measurements (Fig. 4). An evaluation of such measurements showed that within experimental accuracy the flux rate was independent of preceeding photolysis for both complement and perforin pores.

Flux measurements were evaluated by fitting Eqn. 1 to the experimental fluorescence recovery curves. The mean values and standard deviations of the flux rate k are compiled in Table II. In the case of complement the flux measurements were only performed with sheep erythrocyte ghosts. The flux through perforin pores, however, was measured in both sheep and human erythrocyte ghosts. The data of Table II show that k depended in a sensitive and reciprocal manner on the molecular size of the fluorescent tracer: For a 3.6-fold increase of the Stokes' radius the mean k-value decreased about 45-fold.

The sample population distributions of k are plotted in Fig. 5. For both complement and perforin pores and

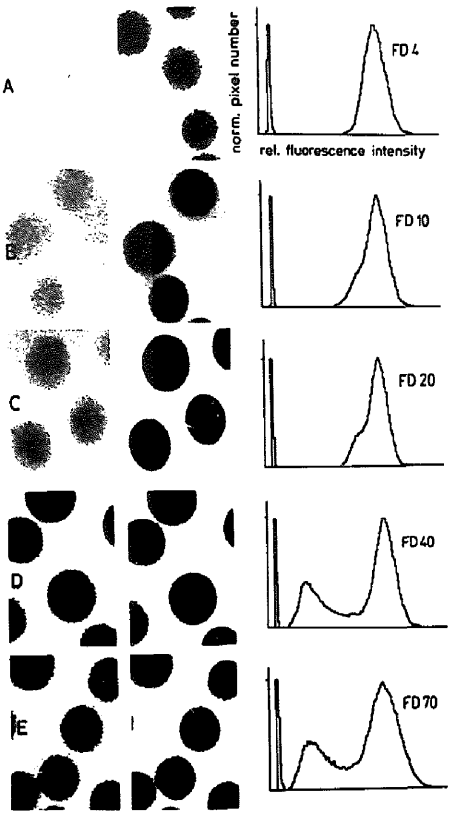

Fig. 2. Exclusion limit of the perforin pore. Resealed human erythrocyte ghosts were treated with perforin and then incubated with FD4 (A), FD10 (B), FD20 (C), FD40 (D), or FD70 (E), respectively, as described in the text. Fluorescence scans were obtained by CLSM before (left) and after (middle) photobleaching. The histograms on the right-hand side represent intensity distributions of the CLSM scans on the left-hand side. The scans and the histograms demonstrate that ghosts are permeable for FD4, FD10 and FD20 but impermeable for FD40 and FD70. In the histograms the peak on the left originates from dark counts, the peak in the center (only D and E) originates from ghosts, while the peak on the right originates from the intensity of the medium (note that only the position of these peaks on the abscissa is significant; the height of the peaks depends on the area density of ghosts). Note that a small degree of bleaching was already introduced by the first scan so that even perfectly permeable ghost appeared slightly darker than background (A–C, left side).

for each of the tracers the distribution of k had a single peak while the standard deviation (assuming approximately normal distributions) was between 30% and 40% of the mean.

The functional radius of the complement and the perforin pore in erythrocyte membranes

The flux measurements showed that the complement pore is permeable to relatively large molecules and has

properties of a molecular sieve with a defined cut-off. It is therefore reasonable to interpret the experimental data in terms of the Renkin-Pappenheimer model (Refs. 44 and 45; for review, see Refs. 46 and 47) which applies to the diffusion of neutral spherical molecules of radius a through a homogeneous population of cylindrical pores of radius r. As discussed previously [48] the functional pore radius can be computed from the flux rate k and the diffusion coefficient D of any two tracers i and j from:

$$[k_i/D_i]/[k_j/D_j] = [E(q_i)F(q_i)]/[E(q_j)F(q_j)] \quad (2)$$

where $E(q) = (1-q)^2$, $F(q) = 1 - 2.104\ q + 2.09\ q^3 - 0.95\ q^5$, and $q = a/r$ [44].

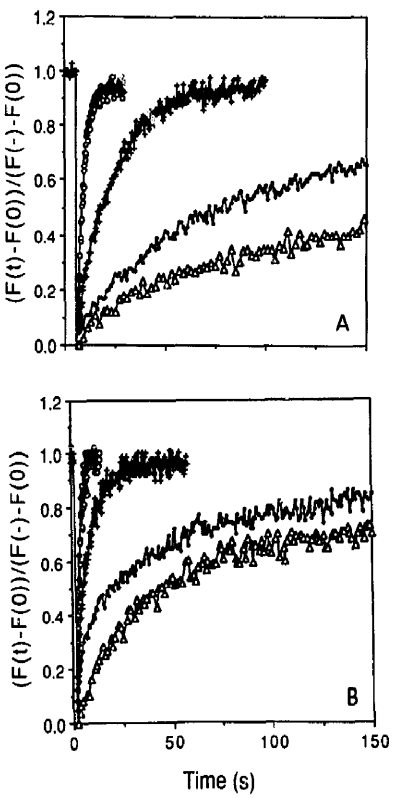

Fig. 3. Effect of molecular size on fluorescent tracer flux through complement and perforin pores. Resealed erythrocyte ghosts were treated with perforin (A) or complement (B), as described. The influx of Lucifer Yellow (○), FD1 (+), FD4 (●) and FD10 (△) into single ghosts was measured by photobleaching. The graphs show representative measurements plotting normalized intracellular fluorescence versus time. The relaxation time of the fluorescence recovery process is inversely proportional to the flux rate k.

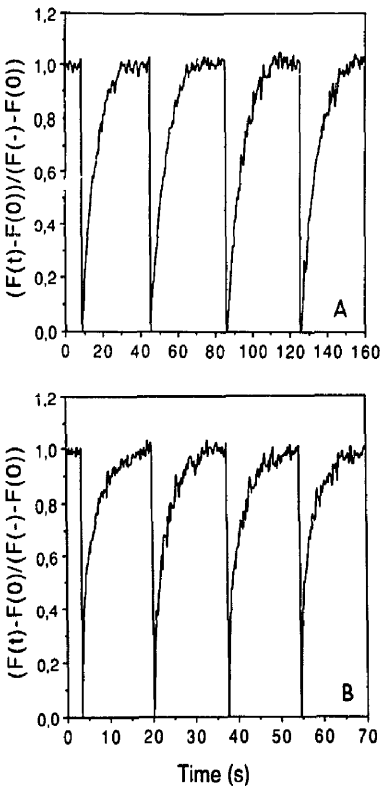

Fig. 4. Test for photochemical damage of complement and perforin pores by photobleaching measurements. Resealed erythrocyte ghosts were treated with perforin (A) or complement (B). Single ghosts were subjected to repetitive photobleaching measurements. The graphs, plotting normalized intracellular fluorescence versus time, give representative examples for the influx of FD1. Evaluation of the flux curves showed that, within experimental accuracy, repetitive photobleaching measurements yielded identical flux rates.

The data of Table II permit to form six different pairs of tracers and thus to calculate, by application of eqn. 2, six different values for the functional pore radius (Table III). In case of the complement pore five out of six values for the pore radius were found in the range between 49.0 Å and 55.8 Å. Only the value calculated for the pair FD4/FD10 is very different, namely 78 Å. It may be noted, however, that this value is the most uncertain one because the difference in the Stokes' radius, flux rate and diffusion coefficient of FD4 and FD10 is markedly smaller than with all other pairs (Table I). The mean pore radius amounts to 57.3 ± 10.5 Å (mean ± S.D.) using all six values, or to 53.1 ± 3.0 Å if the value for the FD4/FD10-pair is omitted. The perforin pore has a radius very similar to that of the complement pore. It was 53.0 ± 1.3 Å for the sheep

erythrocyte membrane and 57.0 ± 4.4 Å for the human erythrocyte membrane.

Effect of a perforin-specific antibody on the permeability of the perforin pore in human erythrocyte membranes

Resealed human erythrocyte ghosts were incubated with perforin, washed, incubated with the perforin-specific antibody, washed again, and then incubated with a fluorescent tracer and subjected to flux measurements. Depending on the concentration of the antibody fluorescent tracer flux was partially but never completely inhibited. These relations are illustrated for FD1 in Fig. 6. For half-maximal inhibition an antiserum dilution of 150-fold was necessary whereas maximal inhibition was achieved by antiserum dilutions of ≤ 100-fold. The maximal degree of inhibition depended on the tracer (Table II). Compared to the control the flux rate was reduced by 20% for Lucifer Yellow, by 47% for FD1, and by 56% for FD4 at high antibody concentrations. This observation is consistent with a reduction of the functional pore radius from the control value of 57.0 ± 4.4 Å to 45.0 ± 2.5 Å (Table III).

For the mechanism of antibody action two extremes seem conceivable. The perforin pores could be heterogeneous with regard to the accessibility of the epitope recognised by the antibody. If the flux through pores recognised by the antibody would be totally blocked the relative degree of flux inhibition would be equal for all tracers and the functional pore radius would not change.

TABLE II

Rate constants of fluorescent tracer flux through complement and perforin pores in membranes of sheep and human erythrocytes and erythroleukemia K-562 cells

Rate constants are given as mean ± S.D. with number of measurements in brackets. SEG, sheep erythrocyte ghost; HEG, human erythrocyte ghost; K-562, K-562 cell line; + AB, preincubation with a perforin-specific antibody (100-fold dilution).

Pore-forming protein	Membrane system	Tracer	Rate constant (10^{-3} s^{-1})
Complement	SEG	LY	555.0 ± 183.0 (33)
		FD1	113.0 ± 46.7 (42)
		FD4	20.4 ± 7.6 (36)
		FD10	12.9 ± 5.2 (33)
Perforin	SEG	LY	1,831.0 ± 674.0 (41)
		FD1	348.8 ± 85.8 (34)
		FD4	71.1 ± 16.8 (38)
		FD10	36.1 ± 8.7 (33)
Perforin	HEG	LY	232.1 ± 86.6 (71)
		FD1	49.9 ± 17.0 (32)
		FD4	10.2 ± 5.5 (73)
		FD10	5.4 ± 2.5 (44)
Perforin	HEG + AB	LY	186.7 ± 75.4 (36)
		FD1	26.4 ± 11.2 (30)
		FD4	4.5 ± 1.4 (39)
Perforin	K-562	FD1	235.0 ± 72.0 (39)
		FD4	48.8 ± 18.1 (43)
		FD10	23.4 ± 7.3 (32)

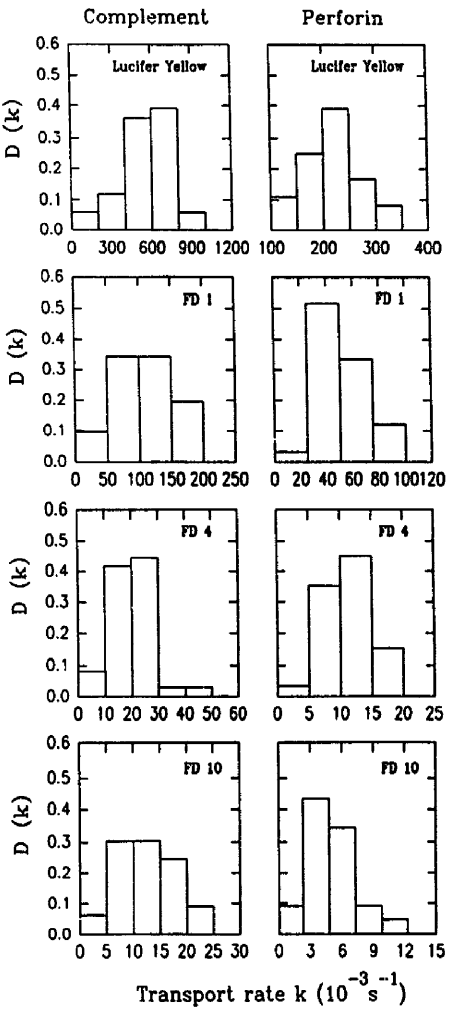

Fig. 5. Sample population distribution of the flux rate. The single-cell flux rate k of Lucifer Yellow (LY), FD1, FD 4 and FD10 was measured in populations of resealed erythrocyte ghosts treated with complement or perforin, as described in the text. The probability density of k, $D(k)$, i.e. the normalized frequency of k per k-interval, was plotted versus k for the various tracers. Each distribution was constructed from 30–70 measurements as specified in Table II.

Alternatively, the antigenic epitope might be uniformly accessible in all perforin pores. In that case each pore could bind an equal maximum number of antibody molecules which would yield an uniform reduction of the functional radius. The fact that the degree of inhibition depended on the Stokes' radius of the tracer and that the flux rates for the different tracers all yielded a similar pore radius strongly argues for uniform antibody binding.

TABLE III

Functional radius of complement and the perforin pores in erythrocyte and K-562 cell membranes

Numbers represent values of the functional pore radius in Å, calculated according to Eqn. 2 from the flux rates and diffusion coefficients of two tracers. SEG, sheep erythrocyte ghost; HEG, human erythrocyte ghost; K-562, K-562 cell line; +AB, preincubation with the perforin-specific antibody (100-fold dilution). n.d., not determined.

Pore-forming protein	Membrane system	1. Tracer	2. Tracer		
			FD1	FD4	FD10
Complement	SEG	LY	54.5	51.0	55.5
		FD1		49.0	55.8
		FD4			78.0
Perforin	SEG	LY	52.0	52.0	53.0
		FD1		52.0	54.0
		FD4			55.0
Perforin	HEG	LY	57.0	54.0	56.5
		FD1		52.0	56.0
		FD4			65.0
Perforin	HEG+AB	LY	42.5	45.0	n.d.
		FD1		47.5	n.d.
Perforin	K-562	FD1	n.d.	53.0	54.0
		FD4			54.0

Permeability and functional radius of the perforin pore in the plasma membrane of intact erythroleukemia cells

K-562 cells were incubated with high concentrations of perforin. In order to prevent colloid osmotic lysis a 110 kDa Dextran (final concentration 0.25 mM) was added to the medium. The results of flux measurements are given in Table II. These were compatible with a functional pore radius of 53.5 Å (Table III).

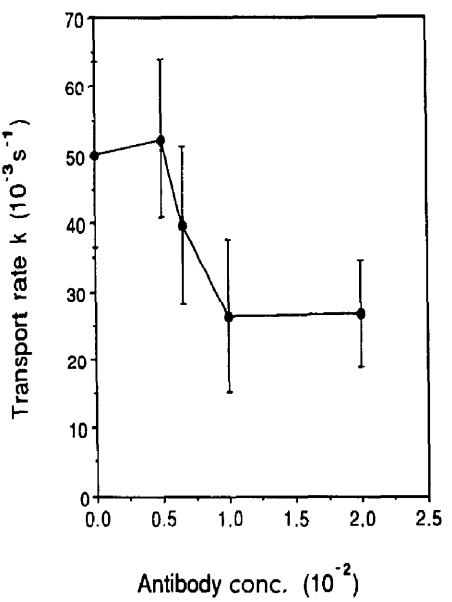

Fig. 6. Effect of a perforin-specific antibody on the transport properties of perforin pores. Resealed human erythrocyte ghosts were treated with perforin as described and then incubated with a perforin specific antibody. The flux rate k of FD1 was measured in relation to the antibody concentration.

Discussion

Previous estimates of the functional radius of the complement pore have varied between 4 and 60 Å

TABLE IV

Previous estimates of the functional radius of complement and perforin pores

ATC, ascites tumor cells; B6.1, B6.1 cell line; EM, electron microscopy; GP, solubilized granule proteins; GPC, guinea pig complement; HC, human complement; HC9, nineth component of human complement; HE, human erythrocyte; HEG, human erythrocyte ghost; HL, human lymphocyte; K-562, K-562 cell line; LB, lipid bilayer; MC, monocytes; ME, mouse erythrocytes; MR, marker release; MSC, mouse spleen cells; NK, cloned mouse Natural Killer cells; OP, osmotic protection; PG, purified granule proteins; PP, purified perforin; RC, rabbit complement; SCC, single-channel conductance; SE, sheep erythrocyte; SEG, sheep erythrocyte ghost; SM, skeletal muscle; YAC-1, YAC-1 cell line.

Effector	Target	Method	Radius (Å)	Ref.
(a) Complement system				
RC	ATC, ME	OP	<35	12
HC	HE	OP	>32.5	13
GPC, HC	HE, SE, *E. coli*	EM	50	21a
RC, GPC	LB	SCC	11	60
C5b-7+GPC	HEG	MR	11.7	16
GPC	SEG	MR	20–25	14
HC	SE	MR	6	17
GPC	SEG	MR	27	15
RC	SM	SCC	4	20
HC	SEG	MR	55	51
GPC			25–35	
HC, GPC	SE	MR	15	49
HC	SE	EM	40–60	21
HC, GPC	SEG	MR	≤19	61
HC	LB	MR	50	62
HC9	LB	SCC	60	18
HC	LB	SCC	15	19
HC9		EM	45	22
(b) Perforin system				
HL	HEG	MR	52–83	63
MC	K-562	EM	77.5	23
NK	YAC-1	EM	80 and 25	53
GP, PP	SE	EM	80 and 35	7
PG	SE	EM	75	64
GP, PP	LB	EM	75	24
PP	HEG	EM	80	5
GP, PP	SE	EM	30–80	4
PG	B6.1	EM	80 and 30	54
PG	HEG	MR	>25	65
GP, PP	LB	SCC	31	55
PG	SE	EM	75–100	66
PP	SE	EM	80	67

(Table IV). Most of this diversity can be attributed to the fact, recognized in the early 1980s, that the size of the complement pore depends on the C9 concentration. It was determined [1,49,50] that, depending on the C9 concentration in the reaction mixture, the number of C9 molecules per complement pore can vary between approximately 1 and 16. Taking this into account both electron microscopic [21a] and functional [51] studies suggest that the maximum internal radius of complement pores is 50–55 Å. The study of perforin pores was delayed by the fact that purified lytic granule proteins and purified perforin became available only recently [4,5,7,52]. Electron microscopic studies repeatedly [23,24,50] suggested that the perforin pore is substantially larger than the complement pore. In some studies [7,53,54] two populations of perforin pores were observed with radii much larger or much smaller, respectively, than that of the complement pore. Recent electrical single-channel recording of perforin and complement pores in planar lipid bilayers suggested [18,55] that the perforin pore is definitely smaller (functional radius 31 Å) than the complement pore (functional radius 60 Å). Our recent fluorescence microscopic single-channel recordings [34] suggested that the perforin pore in human erythrocyte membranes has a functional radius close to 50 Å and that the pore radius, within wide limits, is independent of the perforin concentration.

Our estimates of the functional pore radius were based on two different methods, the exclusion limit and the dependence of the flux rate on molecular size. Relying on hydrodynamic principles the evaluation of flux rates according to Pappenheimer and Renkin holds only for the diffusion of hydrophilic hard spheres through a homogeneous population of cylindrical water-filled pores which perpendicularly traverse the membrane. In spite of these somewhat unnatural conditions the application of the Pappenheimer-Renkin equations seems to be well justified in the present case because electron microscopic studies clearly showed that both complement and perforin pores are large cylinders traversing the membrane perpendicularly [21a,23]. Furthermore, our calculations were self-consistent in that the pairing of tracer data yielded similar pore radii. Nevertheless, it is reassuring that both the Pappenheimer-Renkin approach and the exclusion limit determinations lead to the same conclusion, namely that complement and perforin pores have functional radii very similar to that of a 40 kDa Dextran, i.e. close to 50 Å.

The present study yielded information about the sample population distribution of k (Fig. 5). Each of the distributions has only one peak. This implies that subpopulations of complement or perforin pores with largely different sizes, e.g. P1 pores with 80 Å and P2 pores with 25–30 Å radius [53], do not occur under the present experimental conditions. The existence of P2 pores has been questioned previously [54]. The standard deviations of the k distributions amounted to about 30–40% of the mean (Fig. 5). One source of this deviation is the variation of N, the number of pores per cell. We have recently determined the single-pore flux rate for both perforin [34] and complement (Sauer et al., unpublished results) pores and therefore can estimate N fairly well at least for perforin. For perforin-treated human erythrocyte ghosts the k of Lucifer Yellow was $232.1 \cdot 10^{-3}$ s^{-1} (Table II) while the k for ghosts with one perforin pore is $4.65 \cdot 10^{-3}$ s^{-1} [34]. Since k is directly proportional to N [34] N can be estimated to be $232.2/4.65 = 49.9$. Furthermore, since the Poisson distribution was shown to apply to the distribution of pores among ghosts [34], the standard deviation of N amounts to $N^{1/2} = (49.9)^{1/2} = 7.1$. Similar considerations may apply to complement pores. Thus, pore number variations alone account for a substantial part (approximately ±15%) of the experimentally observed (±30–40%) standard deviation of k. The remainder may be mostly contributed by a variability in the number complement or perforin monomers per pore. If the mean number per pore of C5, C6, C7, C8 and C9 monomers on the one hand or perforin monomers on the other is approximately 15 [7,22,50] a variation of, for instance, +2 monomers per pore would yield a ±13% variation of the pore circumference and a ±28% variation of both the pore cross section and the k value. Without going into further statistical details these considerations permit the conclusion that the experimentally observed distributions of k are only consistent with a small degree of pore size heterogeneity, e.g. with a pore composition of approximately 15 ± 1–2 complement or perforin monomers.

Both complement and perforin pores are assembled from monomeric components. Therefore, the composition and size of the final transmembrane pore may possibly be influenced by structural and dynamic membrane properties, in particular by the lateral mobility of integral membrane proteins. The erythrocyte membrane is an extreme case in this respect because its spectrin-actin skeleton severely restricts protein lateral mobility. Integral erythrocyte membrane proteins such as band 3 and glycophorin are virtually immobile, i.e. their apparent lateral diffusion coefficient is in the range of $10^{-12} - 10^{-11}$ cm^2/s [56]. Cells other than erythrocytes display more 'fluid' membranes with protein lateral diffusion coefficients of 10^{-10}–10^{-9} cm^2/s [57–59]. It was therefore of interest to compare the functional size of perforin pores in erythrocyte membranes with that in the plasma membrane of highly undifferentiated cultured cells. However, our measurements showed that the size of the perforin pore is virtually independent of the cell type. Whether the same applies for complement pores has yet to be determined.

Acknowledgements

This study was supported by a grant of the Deutsche Forschungsgemeinschaft to R.P.

References

1 Bhakdi, S. and Tranum-Jensen, J. (1987) Rev. Physiol. Biochem. Pharmacol. 107, 148–223.
2 Mayer, M.M. (1972) Proc. Natl. Acad. Sci. USA 69, 2954–2958.
3 Bhakdi, S. and Tranum-Jensen, J. (1984) J. Immunol. 133, 1453–1463.
4 Masson D. and Tschopp, J. (1985) J. Biol. Chem. 260, 9069–9072.
5 Podack, E.R., Young, J.D.E. and Cohn, Z.A. (1985) Proc. Natl. Acad. Sci. USA 82, 8629–8633.
6 Tschopp, J., Schäfer, S., Masson, D., Peitsch, M. and Heusser, C. (1989) Nature (Lond.) 337, 272–274.
7 Podack, E.R. and Konigsberg, P.J. (1984) J. Exp. Med. 169, 695–710.
8 Kwon, B.S., Wakulchik, M., Liu, C.C., Persechini, P.M., Trapani, P.M., Kim, A.K. and Young, J.D.-E. (1989) Biochem. Biophys. Res. Commun. 158, 1–10.
9 Shinkai, Y., Takio, K. and Okomura, K. (1988) Nature (Lond.) 334, 525–527.
10 Lichtenheld, M.G., Olsen, K., Lu, P., Lowrey, D.M.., Hameed, A., Hengartner, H. and Podack, E.R. (1988) Nature (Lond.) 335, 448–451.
11 Stanley, K. and Luzio, P. (1988) Nature (Lond.) 334, 475–476.
12 Green, H., Barrow, P. and Goldberg, B. (1959) J. Exp. Med. 110, 699–712.
13 Sears, D.A., Weed, R.I. and Swisher, S.N. (1964) J. Clin. Invest. 43, 975–985.
14 Giavedoni, E.B., Chow, Y.M. and Dalmasso, A.P. (1979) J. Immunol. 122, 240–245.
15 Ramm, L.E. and Mayer, M.M. (1980) J. Immunol. 124, 2281–2287.
16 Sims, P.J. and Lauf, P.K. (1978) Proc. Natl. Acad. Sci. USA 75, 5669–5673.
17 Li, C.K.N. and Levine, R.P. (1980) Mol. Immunol. 17, 1465–1474.
18 Young, J.D.-E., Cohn, Z.A. and Podack, E.R. (1986) Science (Wash.) 233, 184–190.
19 Benz, R., Schmid, A., Wiedmer, T. and Sims, P. (1986) J. Membr. Biol. 94, 37–45.
20 Jackson, M.B., Stephens, C.L. and Lecar, H. (1981) Proc. Natl. Acad. Sci. USA 78, 6421–6425.
21 Tranum-Jensen, J. and Bhakdi, S. (1983) J. Cell Biol. 97, 618–626.
21 (a) Humphrey, J.H. and Dourmashkin, R.R. (1969) Adv. Immunol. 11, 75–115.
22 DiScipio, R.G. and Hugli, T.E. (1985) J. Biol. Chem. 260, 14802–14809.
23 Dourmashkin, R.R., Deteix, P., Simone, C.B. and Henkart, P. (1980) Clin. Exp. Immunol. 42, 554–560.
24 Blumenthal, R., Millard, P.J., Henkart, M.P., Reynolds, C.W. and Henkart, P.A. (1984) Proc. Natl. Acad. Sci. USA 81, 5551–5555.
25 Bashford, C.L., Menestrina, G., Henkart, P.A. and Pasternak, C. (1988) J. Immunol. 141, 3965–3974.
26 Young, J.D.-E., Damiano, A., DiNome, M.A., Leong, L.G. and Cohn, Z.A. (1987) J. Exp. Med. 165, 1371–1382.
27 Wilson, T. and Sheppard, C. (1984) Theory and practice of scanning optical microscopy, pp. 1–213, Academic Press, London.
28 Brakenhoff, G.J., Von Spronsen, E.A., Van der Voort, H.T.M., and Nanninga, N. (1989) Methods Cell Biol. 30, 379–398.
29 Peters, R., Peters, J., Tews, K.H. and Bähr, W. (1974) Biochim. Biophys. Acta 367, 282–294.
30 Edidin, M., Zagyansky, Y. and Lardner, T.J. (1976) Science (Wash.) 191, 466–468.
31 Jacobson, K., Wu, E.-S. and Poste, G. (1976) Biochim. Biophys. Acta 433, 215–222.
32 Axelrod, D., Koppel, D.E., Schlessinger, J., Elson, E. and Webb, W.W. (1976) Biophys. J. 16, 1055–1069.
33 Peters, R. (1983) J. Biol. Chem. 258, 11427–11429.
34 Peters, R., Sauer, H., Tschopp, J. and Fritzsch, G. (1990) EMBO J. 9, 2447–2451.
35 DeBelder, A.N. and Granath, K. (1973) Carbohydr. Res. 30, 375–378.
36 Schwoch, G. and Passow, H. (1973) Mol. Cell Biochem. 2, 975–985.
37 Lozzio, C.B. and Lozzio, B.B. (1975) Blood 45, 321–333.
38 Tschopp, J., Schäfer, S. and Masson, D. (1986) J. Immunol. 137, 1950–1953.
39 Peters, R. and Scholz, M. (1990) in New techniques of optical microscopy and microspectroscopy (Cherry, R.E., ed.,) pp. 199–228, Macmillan, London.
40 Garland, P. (1981) Biophys. J. 33, 481–482.
41 Scholz, M., Schulten, K. and Peters, R. (1985) Eur. Biophys. J. 13, 37–44.
42 Akeson, S.P. and Mel, H.C. (1982) Biochim. Biophys. Acta 718, 201–211.
43 Blunt, M.H. (1975) The blood of sheep, pp. 33–34, Springer, Berlin.
44 Pappenheimer, J.R., Renkin, E.M. and Borrero, L.M. (1951) Am. J. Physiol. 167, 13–21.
45 Renkin, E.M. (1953) J. Gen. Physiol. 38, 225–243.
46 Renkin, E.M. and Curry, F.E. (1979) in Transport Organs (Giebisch, G., ed.), pp. 1–45, Springer, Berlin.
47 Peters, R. (1986) Biochim. Biophys. Acta 864, 305–359.
48 Peters, R. (1984) EMBO J. 3, 1831–1836.
49 Ramm, L.E., Whitlow, M.B. and Mayer, M.M. (1982) Proc. Natl. Acad. Sci. USA 79, 4751–5755.
50 Podack, E.R., Tschopp, J. and Müller-Eberhard, H.J. (1982) J. Exp. Med. 156, 268–282.
51 Dalmasso, A.P. and Benson, B.A. (1981) J. Immunol. 127, 2214–2218.
52 Henkart, P.A. (1985) Annu. Rev. Immunol. 3, 31–58.
53 Podack, E.R. and Dennert, G. (1983) Nature (Lond.) 302, 442–445.
54 Masson, D., Corthesy, P., Nabholz, N. and Tschopp, J. (1985) EMBO J. 4, 2533–2538.
55 Young, J.D.-E., Hengartner, H., Podack, E.R. and Cohn, Z.A. (1986) Cell 44, 849–859.
56 Peters, R. (1988) FEBS Lett. 234, 1–7.
57 Peters, R. (1981) Cell Biol. Intern. Rep. 5, 733–760.
58 Edidin, M. (1987) Curr. Top. Membr. Transp. 29, 91–127.
59 Jacobson, K., Ishihara, A. and Inman, R. (1987) Annu. Rev. Physiol. 49, 163–175.
60 Wobshall, D. and McKeon, C. (1975) Biochim. Biophys. Acta 413, 317–321.
61 Ramm, L.E., Whitlow, M.B. and Mayer, M.M. (1985) J. Immunol. 134, 2594–2599.
62 Malinski, J.A. and Nelsestuen, G.L. (1989) Biochemistry 28, 61–70.
63 Simone, C.B. and Henkart, P. (1980) J. Immunol. 124, 954–963.
64 Henkart, P.A., Millard, P.J., Reynolds,C.W. and Henkart, M.P. (1984) J. Exp. Med. 160, 75–93.
65 Criado, M., Lindstrom, J.M., Anderson, C.G. and Dennert, G. (1985) J. Immunol. 135, 4245–4251.
66 Young, J.D.-E., Nathan, C.F., Podack, E.R., Palladino, M.A. and Cohn, Z.A. (1986) Proc. Natl. Acad. Sci. USA 83, 150–154.
67 Tschopp, J. and Jongeneel, C.V. (1988) Biochemistry 27, 2641–2646.